Properties of Polyetherimide/Dicyanate Semi-interpenetrating Polymer Network Having the Morphology Spectrum

Yu-Seung Kim and Sung-Chul Kim*

Department of Chemical Engineering, Korea Advanced Institute of Science and Technology, Kusongdong Yusongku, Taejon 305-701, Korea

Received July 10, 1998; Revised Manuscript Received December 9, 1998

ABSTRACT: The morphology, tensile properties, and fracture behavior of polyetherimide (PEI)/dicyanate semi-interpenetrating polymer networks (semi-IPNs) with a morphology spectrum were analyzed. Semi-IPNs with a morphology spectrum were prepared by inserting PEI film into neat dicyanate resin, by controlling the relative rate of the dissolution and diffusion of the inserted PEI film, and by controlling the curing reaction of the dicyanate resin using a zinc stearate catalyst. The morphology spectrum was obtained by the accompanied phase separation during curing. Final morphology of the cured dicyanate revealed three types of morphology along thickness direction because of the PEI concentration gradient formed: (1) nodular spinodal structure where the concentration of PEI was 18 wt % or more; (2) dual-phase morphology having both sea-island region and nodular structure where PEI concentration was about 15 wt %; (3) sea-island morphology where PEI concentration was 12 wt % or less. Semi-IPNs with the morphology spectrum displayed improved tensile properties in IPNs with the overall PEI content less than 15 wt %. In addition, semi-IPNs with 7.5 wt % PEI having the morphology spectrum showed a critical strain energy release rate, G_{IC}, of 0.61 kJ/m^2, which was 2.1 times that of the IPNs having uniform single morphology (sea-island structure). It was found that the tensile strength and the fracture toughness enhancement were proportional to the layer thickness having nodular structure and/or dual-phase morphology.

Introduction

Thermosetting materials such as epoxy resins are currently used in many applications that require high modulus and strength, low creep, and high performance at elevated temperatures. The widespread use of the thermosets, however, is limited in many high-performance applications because of their inherent brittleness. Several methods have been proposed to improve the fracture toughness of thermosetting networks. Among them, incorporation of high-performance thermoplastics has been recently highlighted as a new approach for enhancing the toughness of thermosets without significantly lowering their thermal and mechanical properties.[1−5]

The degree of toughening of thermoplastic modified thermosets is strongly dependent on the phase-separated morphology.[6−9] Generally, at low thermoplastic contents (typically below 10 wt %), the thermoplastic-rich phase segregates into spherical domains within the thermoset continuous phase, resulting in a moderate increase in fracture toughness. This is called sea-island morphology, which is formed via the nucleation and growth (NG) mode of the phase separation mechanism. Above 20 wt %, a nodular structure is developed via the spinodal decomposition (SD) mechanism of the phase separation in which the thermoset-rich phase forms interconnected spherical nodules in the thermoplastic matrix. This nodular spinodal structure produces a substantial increase in fracture toughness because of the large capacity for plastic deformation of the thermoplastic-rich phase.[3,4,10,11]

However, thermoset materials with high thermoplastic modifier content often display poor heat and solvent resistance[5,12] as well as the processing difficulties caused by the high viscosity of the mixture. In addition, thermoplastic modifiers usually cost more than thermoset resins. Thus, it is necessary to develop new methods for toughening thermoset materials with low thermoplastic concentrations.

In our previous study, it was found that the concentration gradients of thermoplastic modifiers resulted in the formation of a morphology spectrum and exhibited higher interlaminar fracture toughness in carbon fiber−dicyanate composites with low concentrations of thermoplastic.[13,14] The morphology spectrum concept may be effectively utilized to toughen brittle thermoset materials, because the concentration gradients developed in thermoset resin resulted in a partially nodular spinodal structure.

In this study, polyetherimide (PEI)/dicyanate semi-IPNs with a morphology spectrum were prepared by controlling the kinetics of dissolution and diffusion of the PEI film, and by controlling the curing reaction of dicyanate. Morphology, tensile properties, and fracture toughness of the semi-IPNs were investigated and compared to control samples having a uniform concentration of PEI in the sample.

Experimental Section

Materials. The thermoset component chosen for this study was bisphenol-A dicyanate (AroCy B-10, Ciba-Geigy), supplied as a white, high-purity (>99.5%) crystalline powder (melting point: 79 °C). The molecular structure of the dicyanate monomer and the trimerization reaction involved during cure are reported in Scheme 1. A zinc stearate (ZnSt) catalyst was used to control the reaction rate of the dicyanate resin. The thermoplastic modifier to toughen the dicyanate was amorphous polyetherimide (PEI) (Ultem 1000, General Electric Co., $\overline{M}_n$ = 18000) with T_g of 210 °C. All materials were used as received from the manufacturer.

Specimen Preparation. The PEI/dicyanate semi-IPNs with a morphology spectrum were prepared by inserting PEI

* To whom correspondence should be addressed.

10.1021/ma981083v CCC: $18.00
Published on Web 03/13/1999

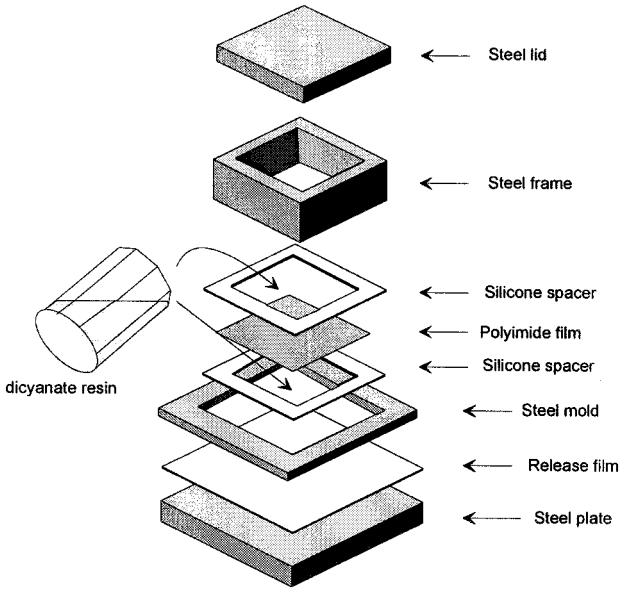

Figure 1. Layout of the casting mold for the formation of the morphology spectrum.

Scheme 1: Molecular Structure of the Dicyanate Monomer and the Trimerization Reaction Involved during Cure

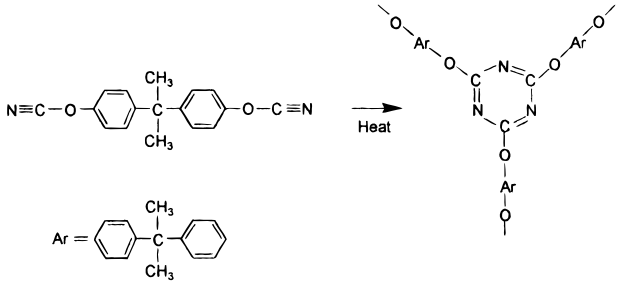

film with designated thickness into the curable dicyanate resin. The PEI was first dissolved in methylene chloride to obtain a 10 wt % solution. This solution was poured on to a clean glass plate and cast by a film applicator. The cast PEI solution was dried at room temperature for 2 h and then heated slowly to 150 °C under vacuum conditions to remove the remaining solvent. For the catalyzed system, 100 or 300 ppm of ZnSt catalyst was added to the dicyanate resin at 100 °C and the mixture was stirred continuously for 2 min. Half of the prepared dicyanate resin was then poured into a steel mold with dimensions of 140 × 140 × 2.5 mm^3, and an opening of 100 × 100 mm^2, as shown in Figure 1. A release film and silicone rubber spacer with a thickness of 1 mm had been placed in the mold before the dicyanate resin was added. The prepared PEI film and the other silicone spacer covered the preinstalled rubber spacer, and the remainder of the dicyanate resin was then poured onto the PEI film. A steel frame with a steel lid was placed on top of the upper silicone rubber spacer to prevent distortion of the spacers at a high curing temperature. The cure schedules employed in this study were as follows: (i) 210 °C/12 h or 180 °C/24 h for the uncatalyzed dicyanate: (ii) 180 °C/12 h for the dicyanate with 100 ppm of ZnSt: (iii) 180 °C/6 h for the dicyanate with 300 ppm of ZnSt. The code names of the samples were designated 180−0−7.5 and 180−100−7.5, representing the curing temperature of 180 °C with 0 and 100 ppm of ZnSt, respectively; the last number of the code denotes the overall composition (wt %) of the PEI in the dicyanate resin. The conversion of each sample was measured by the differential scanning calorimetry (DSC) and confirmed to be over 80%, which far exceeded the gel point.[15] Post curing of all specimens was performed in a convection oven at 280 °C for 1.5 h. The overall composition of the PEI was calculated based on the areal weight of the PEI film and the weight of the cured specimen. For comparison, 10 control samples of the semi-IPNs with uniform concentration, namely, PEI wt % = 0, 2.5, 5, 7.5, 10, 12.5, 15, 17.5, 20, and 25, were prepared by conventional solution-mixing techniques[9] under the same curing conditions. The dimensions of all specimens were 70 × 70 × 2 mm^3.

Cure Kinetics. Conversion of the dicyanate was determined by using a du Pont 2010 DSC. The heat flow of the dicyanate resin was measured as a function of time for three different catalyst levels of 0, 100, and 300 ppm, respectively, when cured at 180 °C. The conversion of dicyanate was determined as $X = H_t/H_T$, where H_t is the accumulated area under the isothermal DSC curve from $t = 0$ to given time per unit weight of dicyanate, and H_T is the total heat of reaction which is determined by integrating the reaction peak of an initial (uncured) sample from 150 to 350 °C. The H_T was found to be 740 J/g.

Characterization of the Concentration Gradient. The concentration gradient of the cured samples was analyzed by using a Nicolet Magna 550 FT-IR spectrometer equipped with an optical microscope. For the calibration curve, a series of absorption spectra of the control samples having a uniform concentration of PEI was obtained using KBr pellets. The absorbance ratio A_{1560}/A_{1720} for the control samples was then calibrated with the PEI concentration. The 1560 cm^{-1} band is characteristic of the triazine group (six-membered rings of alternating C−N bonds) and was used as the internal standard; the 1720 cm^{-1} band is the characteristic band of the imide group. For the morphology spectrum system, the characteristic band ratio along the thickness of the sample was converted to the PEI content using the calibration curve. Operating conditions for obtaining the spectra involved 128 scans at a resolution of 4 cm^{-1}.

Morphology. The morphologies of the specimen were examined using a Philips 535M scanning electron microscopy (SEM). The fracture surfaces of the semi-IPN were coated with a thin layer of a gold−palladium alloy. The average domain size of the PEI-rich domain and the dicyanate nodule were determined from SEM micrographs.

Mechanical Properties. The mechanical properties of the cured resins were measured with an Instron model 4202 universal-testing machine. Tensile properties were measured with dumbbell shaped microtensile specimens according to ASTM 638-94. The nominal strain rate at the start of the tensile test was 0.1 mm/min.

The critical stress intensity factors, K_{IC}, of the cured semi-IPNs were measured using single-edge-notch geometry as described in ASTM E399-78a. The specimens were cut into rectangular strips 60 mm long, 6 mm wide, and 2 mm thick. An edge crack was made in each rectangular bar, with special care being taken to ensure that the crack plane was perpendicular to the specimen's long axis. The edge crack was made by notching the specimen with a diamond wheel and tapping a sharp blade within the notch. Crack lengths were in the 1.5−3 mm range. The prepared cracked specimens were then loaded into a three point bending fixture with a span length of 24 mm. The concentration gradient was developed along the direction of specimen thickness. Crosshead speed was 1 mm/min. At critical load, P_C, the crack began to propagate and the test was terminated. A minimum of seven specimens was tested for each PEI composition and curing condition. Measured K_{IC} values were converted to critical strain energy release rates, G_{IC} using the following relationship:

$$G_{IC} = \frac{K_{IC}^2}{E}(1 - \nu^2) \qquad (1)$$

where Poisson's ratio ν was taken as 0.35 for all materials and E is Young's modulus.

Results and Discussion

Formation of Morphology Spectrum. The morphology of PEI/dicyanate semi-IPNs depends on the

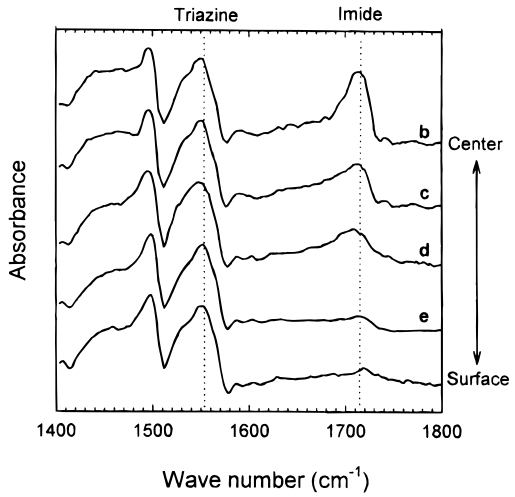

Figure 2. FT-IR absorption spectra of 180−100−7.5 semi-IPNs with the following locations: (b) and (c) region showing nodular structure; (d) region showing dual-phase morphology; (e) region showing sea-island morphology. (The spectra were normalized with the characteristic band of triazine group.)

overall PEI content and curing condition. The phase separation mechanism and the corresponding morphology of the control samples having uniform concentration have been reported in previous studies.[15,16] It was shown that, for a PEI content of less than 14 wt %, the semi-IPNs exhibited a sea-island morphology in which the spherical domains of the PEI-rich phase were distributed within the dicyanate matrix formed via the nucleation and growth (NG) mechanism. At above 19 wt % PEI content, phase separation proceeded via a spinodal decomposition (SD) mechanism and a nodular structure was formed in which the dicyanate phase formed interconnected spherical nodules in the PEI-rich continuous phase. At PEI contents between 14 and 19 wt %, a dual-phase morphology was observed. This morphology was formed via a primary SD mechanism that proceeded to the late stage of phase separation because of the fast diffusion rate with low viscosity of the reaction mixture to give macroscale domains of the PEI-rich and dicyanate-rich phases. The continued curing caused the secondary phase separation from the primarily formed domains of the PEI-rich phase (via the SD mechanism) and dicyanate-rich phase (via the NG mechanism) to give the dual-phase structure.

The control samples prepared by the solution mixing technique exhibited a single type of morphology; however, the semi-IPNs prepared by inserting PEI film into dicyanate resin displayed a morphology spectrum, because of the concentration gradient developed by restricted diffusion of the PEI film during the curing of the dicyanate resin.

Figure 2 represents the FT-IR absorbance spectra of a typical morphology spectrum system containing 7.5 wt % PEI overall concentration and cured at 180 °C with a ZnSt catalyst of 100 ppm (i.e., 180−100−7.5). As the point of measurement on the cross-section of the specimen was moved from surface to center, absorbance at 1720 cm^{-1}, which originated in the imide group, gradually increased.

Figure 3 shows the concentration gradient measured by FT-IR analysis and the corresponding morphology spectrum. Nodular structure (Figure, parts b and c), dual-phase morphology (Figure 3, parts d-1 and d-2), and sea-island morphology (Figure 3e) were observed in sequence as the concentration of PEI decreased from 21.5 to 9 wt %. We observed the sea-island morphology where the PEI-rich phase forms spherical domains with diameters of about 1 μm in the dicyanate matrix in the regions with 1.5∼12 wt % of PEI (see Figure 3e). Besides, some white lines due to the welt formation of the brittle fracture were found in the sea-island morphology. Nodular spinodal structure was observed in regions having 18∼21.5 wt % of PEI. The size of the dicyanate nodules in the nodular structure gradually decreased as the PEI concentration increased toward the center of the specimen (3c → 3b in Figure 3). This is due to the increase in the viscosity of the reacting mixture as the PEI concentration increased, which restricted the rate of phase separation. Consequently, the semi-IPNs with the morphology spectrum exhibited a gradual decrease in the nodule size as the PEI concentration increased. Dual-phase morphology exhibiting the sea-island region and nodular structure was found in the range of 12∼18 wt % of PEI content. In the region showing the dual-phase morphology, large dicyanate-rich domains with a diameter of about 100 μm were surrounded by the PEI-rich domains showing nodular structures (Figure 3d-1); inside the dicyanate-rich domain, small PEI domains with a diameter of about 0.8 μm were formed (Figure 3d-2). The boundary between the nodular structure region and the dual-phase region is clearly seen by the sudden drop in dicyanate nodules, as seen in the top of Figure 3d-1. It is evident that the morphology spectrum obtained in the concentration gradient system corresponds well with the morphologies of the control samples having uniform concentration.

Another noteworthy observation is the boundaries between different morphology layers. Boundaries between the sea-island morphology regions and the dual-phase morphology regions were distinct and straight (boundary A in Figure 3a), while the boundaries between the nodular structures and the dual-phase morphologies were obscure and irregular (boundary B in Figure 3a). Considering the fact that the sea-island morphology formed via the NG mode of phase separation, while the dual-phase morphologies and the nodular structures were formed predominantly in the SD mode, the distinct boundaries were generated from different phase separation mechanisms. The irregular boundaries between the dual phase and the nodular structures were caused by secondary phase separation after the SD mode of phase separation.

Layer Thickness of the Morphology. Variations in layer thickness of the morphology can be achieved either by changing the initial film thickness or controlling curing conditions. Table 1 summarizes the layer thickness, when prepared by varying the film thickness or adding a catalyst. The layer thickness was determined directly from SEM micrographs. When the curing conditions and specimen geometry were maintained constant, the region of nodular structure and/or dual-phase regions increased linearly as the initial thickness of the PEI increased. At 2.5 wt % of overall PEI concentration, neither the nodular structure nor the dual-phase morphology was found because the inserted PEI film was so thin that it was dissolved and diffused thoroughly into the dicyanate resin during cure. In other words, the proper concentration gradient to obtain the nodular structure was not developed. When the overall PEI content was over 2.5 wt %, however, three types of morphology, sea island, dual phase, and nodular structure, were formed.

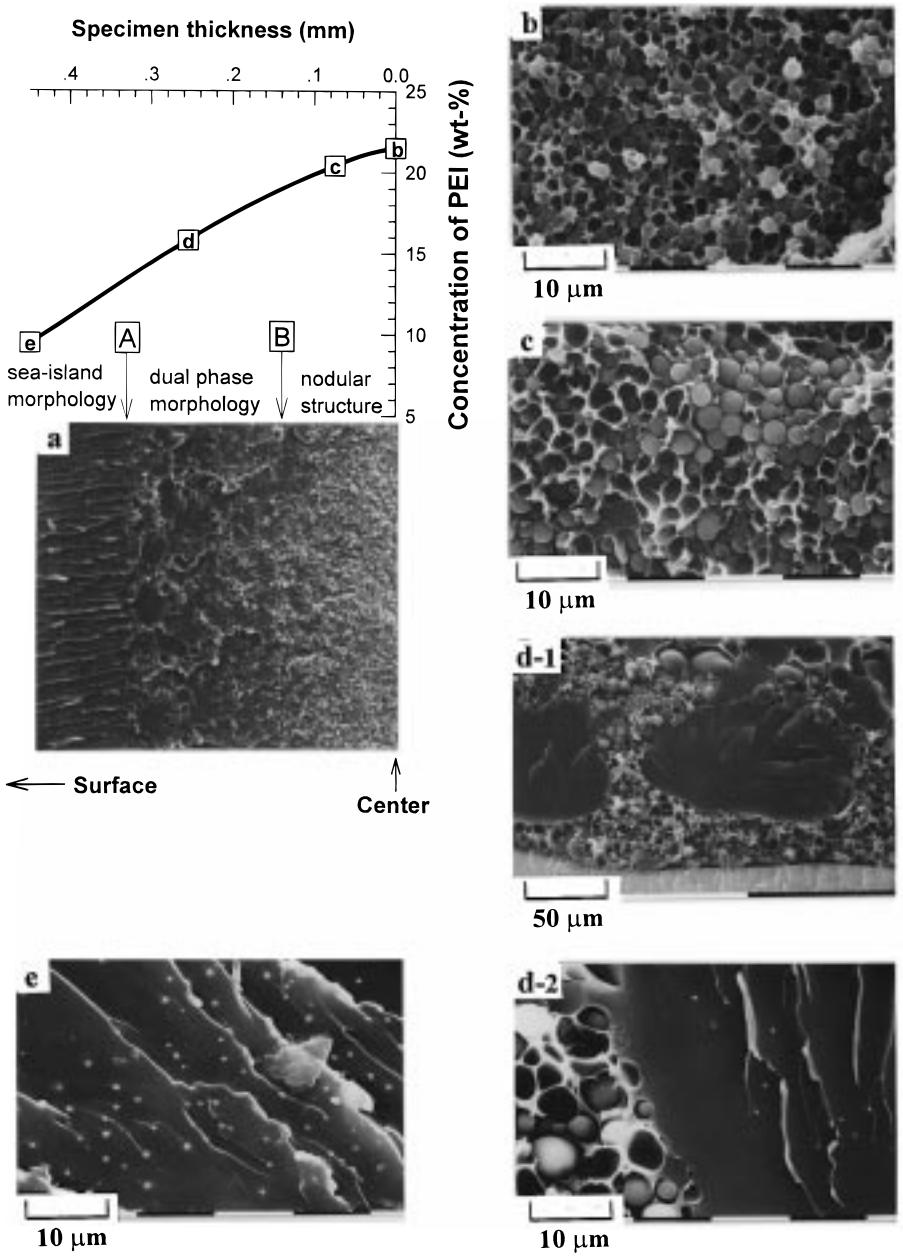

Figure 3. SEM micrographs of the fracture surface of 180−100−7.5 semi-IPNs: (a) low magnification; (b) and (c) nodular structure; (d-1) and (d-2) dual-phase morphology; (e) sea-island morphology.

Curing conditions, such as the curing temperature or the catalyst concentration, are also important factors in controlling the layer thickness of morphologies. In the study, we used ZnSt as the catalyst for accelerating the curing reaction of the dicyanate. Figure 4 shows the conversion changes and changes in gel time with different ZnSt concentrations. The gel time was taken as the time to reach the theoretical gel conversion of 0.6.[17] As the level of ZnSt increased, the curing reaction accelerated considerably, contributing to the shortening of gel time accompanied by the increase in the system viscosity to prevent PEI molecules from diffusing into the dicyanate resin.

Figures 5 and 6 show the concentration gradients and corresponding morphologies at various levels of ZnSt. For 300 ppm of ZnSt, the PEI concentration exhibited a narrow gradient from 58 to 0 wt %. In this case, relatively narrow regions showing the nodular structure and the sea-island morphology were found; a large region showing no morphology was also found outside

Table 1. Initial Film Thickness and the Layer Thickness of Morphology for PEI/Dicyanate Semi-IPNs with a Morphology Spectrum

		layer thickness (mm)	
code	initial film thickness[a] (mm)	sea-island morphology	dual-phase and/or nodular structure[b]
210-0-2.5	0.047	2.0	
210-0-5	0.096	1.65	0.35
210-0-7.5	0.143	1.46	0.54
210-0-10	0.191	1.30	0.70
210-0-12.5	0.240	1.05	0.95
210-0-15	0.288	0.83	1.17
210-0-17.5	0.336	0.66	1.34
180-0-7.5	0.143	1.91	0.09
180-100-7.5	0.143	1.38	0.62
180-300-7.5	0.143	0.80	0.35

[a] The thickness of all specimens is 2 mm. [b] Since the boundary between the dual-phase morphology and nodular morphology was irregular, the summation of each volume fraction could be calculated.

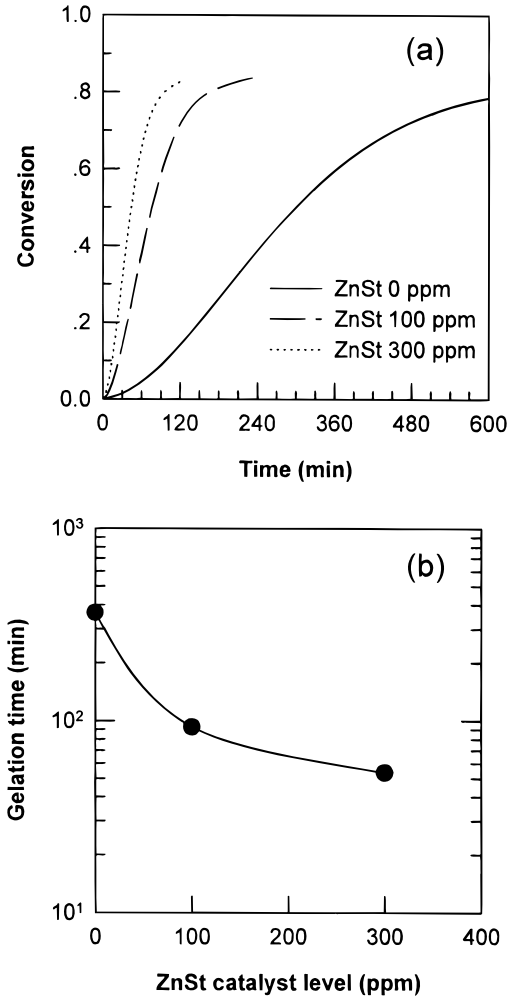

Figure 4. Change of dicyanate conversion (a) and gelation time (b) with different ZnSt catalyst contents (curing temperature was 180 °C).

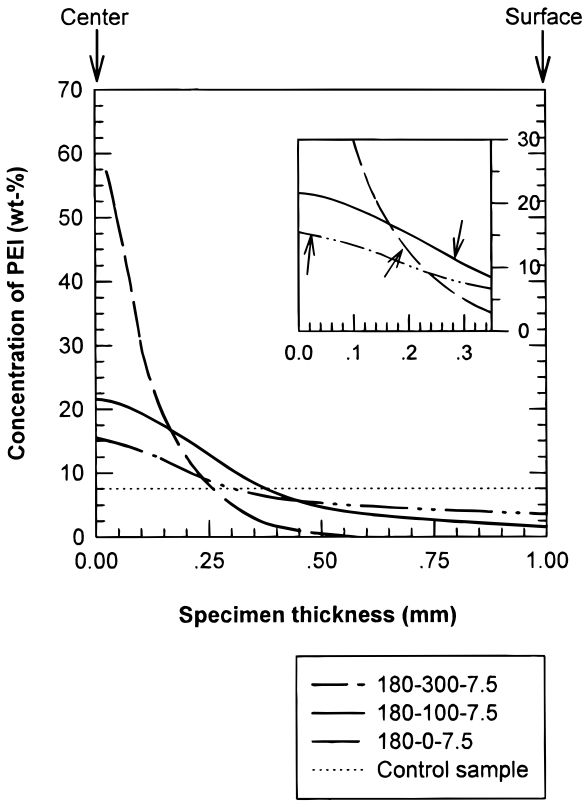

Figure 5. Concentration gradient obtained by FT-IR analysis for the morphology spectrum system with different ZnSt catalyst levels (overall composition of PEI was 7.5 wt %, the arrows locate the concentration where dicyanate nodules appeared): (– – -) 180−300−7.5; (—) 180−100−7.5; (—••—) 180−0−7.5; (•••) control.

the sea-island region (about 0.4 mm from the surface of the specimen had no PEI). However, dual-phase morphology was not observed. It is assumed that the region for the dual-phase morphology was so small that it could not exist as a separate layer. For 100 ppm of ZnSt, relatively large regions of nodular structure and dual-phase and sea-island regions were observed, as described above. For the no-catalyst system, a narrow region showing dual-phase morphology and a large region showing sea-island morphology were found, since the concentration gradient of PEI was broad.

The average domain size of the PEI-rich domain and the dicyanate nodule decreased as the level of ZnSt increased (Table 2). This is due to the high viscosity of the reaction mixture caused by the short gel time. The high viscosity of the mixture reduced the rate of coalescence in the late stage of phase separation.

Tensile Properties. Tensile properties of the control samples and the morphology spectrum system are plotted as a function of the overall PEI content as shown in Figure 7. For the control sample, the tensile strength and elongation at the break were strongly dependent upon morphology, showing dramatic change near the composition of 15 wt % PEI where the dual-phase morphology appeared, while the tensile modulus remained constant, since the two components have similar modulus values. In particular, the tensile strength of the control sample showed a minimum value in the sea-island region, and a distinct increase when the morphology changed to the dual-phase morphology and nodular structure.

The reduction in tensile strength observed in the sea-island region is ascribed to the lack of interfacial adhesion between the PEI-rich domain and the dicyanate matrix, involving no chemical interaction between the inclusion and the matrix. The same phenomenon has been reported in other blend systems.[18−20] When PEI concentration was higher than 12.5 wt %, tensile strength increased significantly, because the two constituents formed co-continuous phases (i.e., dual-phase morphology or nodular structure).

In the morphology spectrum system, tensile strength and elongation at the break increased gradually with increasing PEI content, and no significant decrease was observed except at 2.5 wt % PEI. For example, the 210−0−7.5 sample led to an increase in tensile strength from 84 to 92 MPa, whereas the control sample containing 7.5 wt-% PEI exhibited a lower tensile strength value of 80 MPa. In contrast, the 210−0−2.5 sample had approximately the same value of 84 MPa as the control sample, as it showed only the sea-island morphology throughout the specimen. The results suggest that the region containing a nodular structure having higher tensile strength caused the enhancement of the tensile strength. Consequently, tensile strength is probably proportional to the layer thickness of the nodular and/or dual-phase morphology. Tensile strength values can now be approximated by the rule of mixing, which

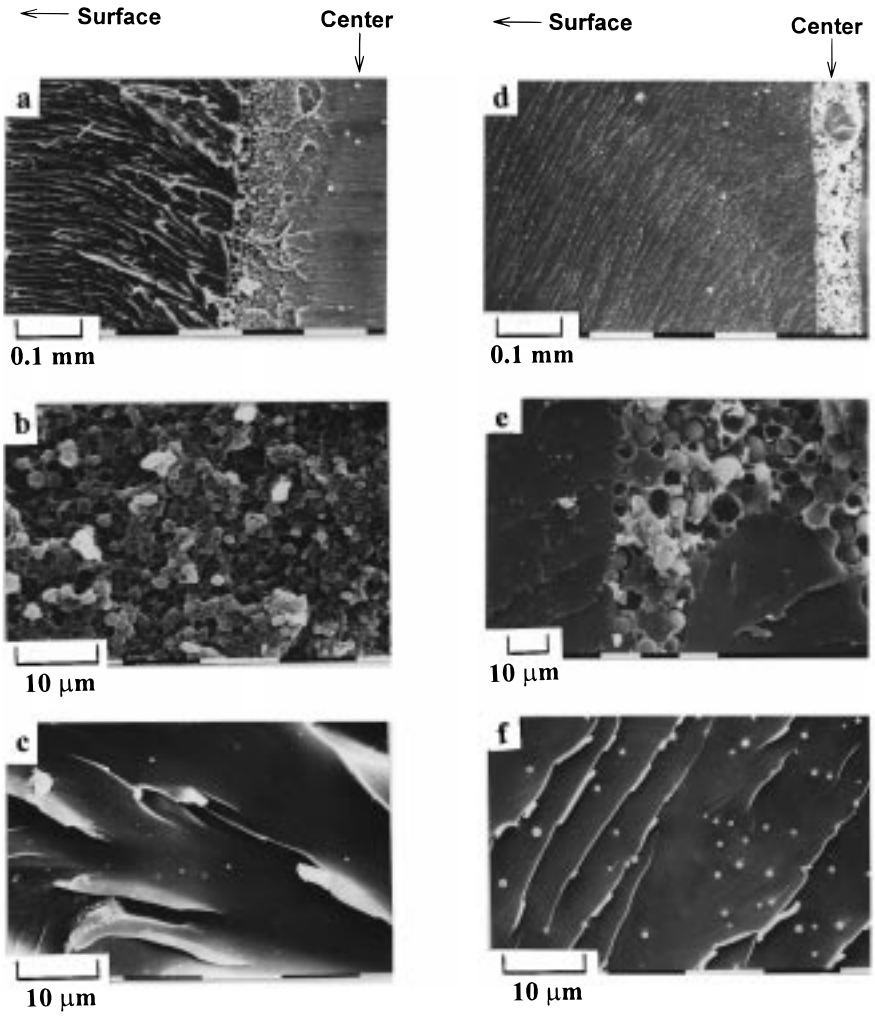

Figure 6. SEM micrographs of the fracture surface of the morphology spectrum system with catalyst levels, 300 ppm of ZnSt: (a) low magnification; (b) region showing nodular structure; (c) region showing sea-island morphology, no catalyst; (d) low magnification; (e) region showing dual-phase morphology; (f) region showing sea-island morphology.

Table 2. Domain Size[a] of the Dispersed Phase Obtained for the Control Sample and Morphology Spectrum System

		sea-island morphology	dual-phase morphology		nodular structure
code	PEI content (wt %)	PEI-rich domain	PEI-rich domain	dicyanate nodule	dicyanate nodule
control sample	2.5	1.34 ± 0.39			
	5	1.22 ± 0.30			
	7.5	1.27 ± 0.28			
	10	1.38 ± 0.30			
	15		1.44 ± 0.32	8.88 ± 1.96	
	20				38.28 ± 8.06
	25				6.32 ± 1.76
	40[b]				1.51 ± 0.34
180−0−7.5	7.5	1.22 ± 0.26	1.48 ± 0.37	6.79 ± 2.99	2.5∼9.6[c]
180−100−7.5	7.5	0.84 ± 0.22	1.03 ± 0.30	4.35 ± 1.30	1.8∼29.2[c]
180−300−7.5	7.5	0.46 ± 0.10			0.2∼14.6[c]

[a] All dimensions are μm and the ± x values show standard deviation. [b] Data taken from Lee.[15] [c] Size of the dicyanate nodules gradually decreased with the concentration of PEI.

assumes parallel coupling of nodular structures and sea-island regions:

$$\sigma(\phi) = (1 - \phi)\sigma_N + \phi\sigma_S \qquad (2)$$

where $\sigma(\phi)$ is the tensile strength of semi-IPNs containing the volume fraction, ϕ, of the sea-island morphology layer: the tensile strength of dual phase and/or nodular structure, σ_N (=112 MPa), and the tensile strength of the sea-island morphology region, σ_S (=83 MPa), were determined by control samples containing the same overall PEI composition.

As shown in Figure 7, the model values using the rule of mixing accurately predicted the tensile strength values. The additive rule of mechanical properties has been observed in microlayer composites having alternating layers of polycarbonate and styrene−acrylonitrile copolymers.[21] The advantage of the tensile strength induced by the morphology spectrum disappeared in

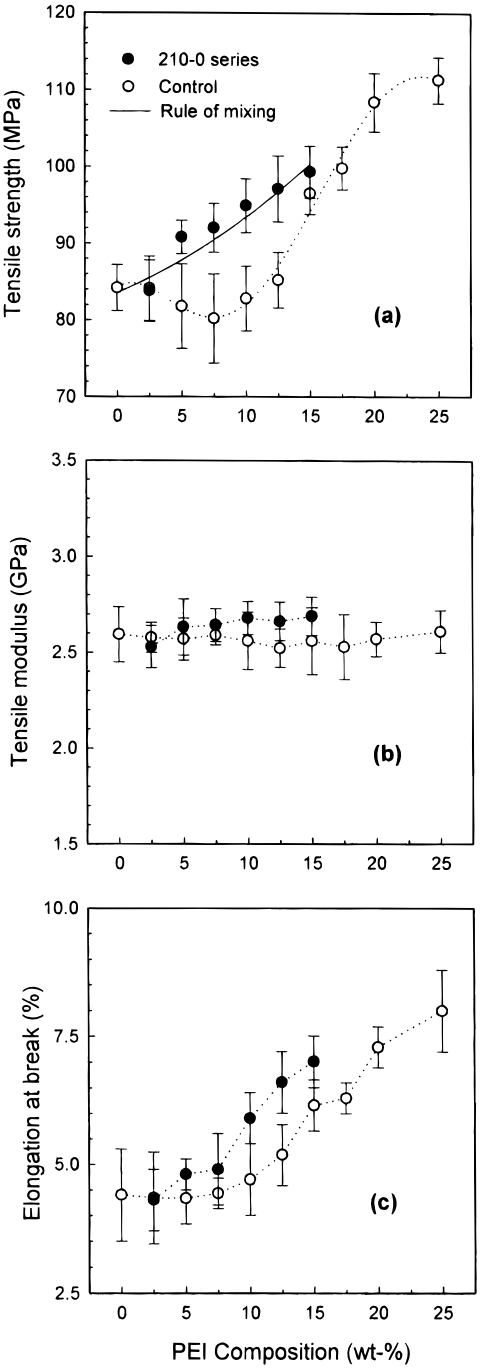

Figure 7. Tensile properties of controls and the morphology spectrum system with PEI composition: (a) tensile strength; (b) tensile modulus; (c) elongation at the break.

compositions where the dual-phase morphology was found, when the overall PEI concentration was higher than 17.5 wt %.

Fracture Toughness. Figure 8 shows the critical strain energy release rates, G_{IC}, for the control samples and the morphology spectrum system as a function of PEI content. For the control samples, at below 15 wt % PEI, G_{IC} increased only slightly, but at 15 wt % or more, it increased substantially. This result can be explained by its morphological features. When the PEI content is less than 15 wt %, and the thermoplastic is located in isolated spherical domains within the dicyanate matrix, (i.e., sea-island morphology), fracture occurs by brittle failure of the dicyanate matrix; the PEI domains bridge the crack and delay its propagation. When the PEI

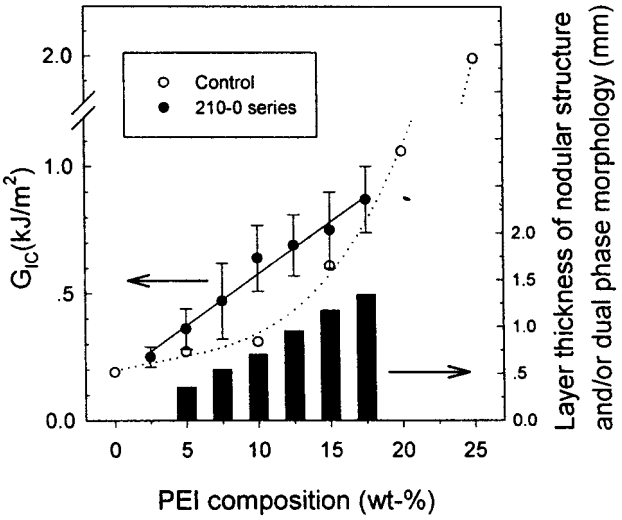

Figure 8. Fracture energy, G_{IC}, of the morphology spectrum system with different PEI contents.

content exceeds 15 wt %, however, a continuous PEI-rich phase forms and the brittle failure changes to a semi-brittle failure with the deformation of the continuous PEI-rich phase around the nodules. Consequently, the fracture toughness of the control sample substantially increases at higher PEI contents.

On the other hand, in the morphology spectrum system, both the brittle failure and the semi-brittle failure occur within the specimens. This is evidenced by the examination of the fracture surfaces, which shows the presence of white streaks (Figure 3a). The texture, which was parallel to the direction of crack growth, were generated in the sea-island morphology, but disappeared at the boundary between sea-island morphology and dual-phase morphology. Considering that the white streaks were usually observed on the fracture surfaces of brittle-natured cross-linked polymers,[23] a brittle-natured fracture occurred in the sea-island region; however, a semi-brittle failure occurred in the nodular structure region. Consequently, the G_{IC} values representing fracture energy reflected a positive effect induced by the plastic deformation of the PEI-rich phase in the nodular structure, as shown in Figure 8.

To clarify the effect of the morphology spectrum on toughness, the strain energy release rate, G_{IC} of the catalyzed system containing 7.5 wt % PEI was measured in terms of the layer thickness of the nodular structure and/or dual-phase morphology. The layer thickness of the morphology was controlled by adding a ZnSt catalyst as described above. Figure 9 shows that the fracture toughness increased as the thickness of the nodular structure and/or dual-phase morphology increased. That is, the highest value of 0.61 kJ/m^2 was obtained in 180−100−7.5 semi-IPNs having 0.62 mm of nodular layer thickness, while the G_{IC} of the control sample without nodular structure was 0.29 kJ/m^2. It was also found that toughness is linearly proportional to the layer thickness of the nodular and/or dual-phase morphology.

Conclusions

The morphology formation, tensile properties, and fracture toughness of PEI/dicyanate semi-IPN with morphology spectrum were investigated. The results led to the following conclusions:

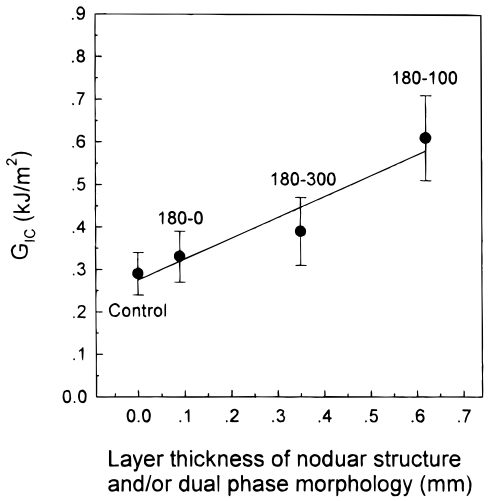

Figure 9. Fracture energy, G_{IC}, of the morphology spectrum system with different catalyst levels.

(1) The final morphology of the cured dicyanate revealed three different types of morphology with PEI concentration: nodular spinodal structure when the concentration of PEI was 18 wt % or more; dual-phase morphology when the PEI concentration was about 15 wt %; sea-island morphology when the concentration of PEI was 12 wt % or less.

(2) The layer thickness of the morphologies linearly increased with initial film thickness and could be controlled by using the ZnSt catalyst, while the overall PEI content remained constant.

(3) Tensile strength and elongation at the break in the morphology spectrum system increased proportionally with the layer thickness of nodular and/or dual-phase morphology. The tensile strength value was consistent with the model by the rule of mixing.

(4) The fracture toughness of the morphology spectrum system was also improved because the toughening effect in the nodular region was superior to that of the sea-island morphology. The G_{IC} of the semi-IPN having 0.62 mm of nodular layer thickness was 0.61 kJ/m^2, which was 2.1 times that of the control sample showing only sea-island morphology.

Acknowledgment. This research was supported by the Center for Advanced Functional Polymer, which was funded by the Korea Science & Engineering Foundation (KOSEF), Taejon, Korea.

References and Notes

(1) Bucknall, C. B.; Gilbert, A. H. *Polymer* **1989**, *30*, 213.
(2) Hedrick, J. L.; Yilgor, I.; Jurek, M.; Hedrick, J. C.; Wilkes, G. L.; McGrath, J. E. *Polymer* **1991**, *32*, 2020.
(3) Pearson, R. A.; Yee, A. F. *Polymer* **1993**, *34*, 3658.
(4) Min, B. G.; Hodgkin, J. H.; Stachurski, Z. H. *J. Appl. Polym. Sci.* **1993**, *50*, 1065.
(5) Woo, E. M.; Shimp, D. A.; Seferis, J. C. *Polymer* **1994**, *35*, 1658.
(6) Bucknall C. B.; Partridge, I. K. *Polym. Eng. Sci.* **1986**, *26*, 54.
(7) Yamanaka, K.; Inoue, T. *Polymer* **1989**, *30*, 662.
(8) Vallo, C. I.; Hu, L.; Frontini, P. M.; Williams, R. J. J. *J. Mater. Sci.* **1994**, *29*, 2481.
(9) Park, J. W.; Kim, S. C. *Polym. Adv. Technol.* **1996**, *7*, 209.
(10) MacKinnon, A. J.; Jenkins S. D.; McGrail, P. T.; Pethrick, R. A, *Macromolecules* **1992**, *25*, 3492.
(11) Bagheri, R.; Pearson. R. A. *J. Mater. Sci.* **1996**, *31*, 3945.
(12) Wertz, D. H.; Prevorsek, D. C. *Polym. Eng. Sci.* **1985**, *25*, 804.
(13) Kim, Y. S.; Kim, S. C. *Makromol. Symp.* **1997**, *118*, 371.
(14) Kim, Y. S.; Kim, S. C. *Polym. Compos.* **1998**, *19*, 714.
(15) Lee, B. K. Ph.D. Dissertation, KAIST, Taejon, Korea, 1995.
(16) Georjon, O.; Galy, J.; Pascault, J. P. *J. Appl. Polym. Sci.* **1993**, *49*, 1441.
(17) Lee, B. K.; Kim, S. C. *Polym. Adv. Technol.* **1995**, *6*, 402.
(18) Kolarik, J. *Polymer* **1994**, *35*, 3631.
(19) Han, C. D.; Villamizar, C. A.; Kim, Y. W. *J. Appl. Polym. Sci.* **1975**, *19*, 2831.
(20) Pukanszky, B.; Tudos, F. *Makromol. Chem., Macromol. Symp.* **1990**, *38*, 221.
(21) Shin, E.; Hiltner, A.; Baer, E. *J. Appl. Polym. Sci.* **1993**, *47*, 269.
(22) Lee, S. S.; Kim, S. C. *J. Appl. Polym. Sci.* **1997**, *64*, 941.
(23) Robertson, R. E.; Mindroiu, V. E. *Polym. Eng. Sci.* **1987**, *27*, 55.

MA981083V